

Electron escape from InAs quantum dots

C. M. A. Kapteyn, F. Heinrichsdorff, O. Stier, R. Heitz, M. Grundmann,
N. D. Zakharov,* and D. Bimberg

Institut für Festkörperphysik, Technische Universität Berlin, Hardenbergstrasse 36, D-10623 Berlin, Germany

P. Werner

Max-Planck-Institut für Mikrostrukturphysik, Weinberg 2, D-06120 Halle, Germany

(Received 29 April 1999; revised manuscript received 16 August 1999)

We identify fundamental mechanisms of electron escape from self-organized InAs quantum dots (QD's) in a vertical electric field by time-resolved capacitance spectroscopy. Direct tunneling and a thermally activated escape process are observed. The QD electron ground and first-excited states are concluded to be located ~ 190 and ~ 96 meV below the GaAs matrix conduction band, respectively. Our experimental results and their interpretation are in good agreement with eight-band $\mathbf{k}\cdot\mathbf{p}$ calculations and demonstrate the importance of tunnel processes. [S0163-1829(99)01344-2]

Quantum dots (QD's) exhibit unique electronic properties due to the ultimate reduction of size in all three dimensions of real space. Over the past few years, they have therefore attracted rapidly growing attention.¹ Self-organization processes during epitaxial growth of highly lattice-mismatched materials, i.e., the Stranski-Krastanow growth mode,² are increasingly employed to form relatively homogeneous ensembles of QD's.³⁻⁵ Their peculiar optical properties^{6,7} and enormous application potential for novel optoelectronic devices such as lasers,⁸⁻¹⁰ detectors,¹¹ and optical memory structures¹²⁻¹⁴ has stimulated additional research interest. For most applications, however, *single-carrier* capture, confinement, and escape play a significant role. Only few related investigations were reported until now, none in an external electric field, and unambiguous interpretation has only recently been facilitated due to progress in the theory of electronic states in QD's.¹⁵⁻¹⁷ This article reports the first direct observation of electron escape from InAs QD's, shedding new light on the physics of the emission mechanisms.

In the case of deep centers and quantum wells (QW's), capacitance spectroscopy and deep-level transient spectroscopy (DLTS),¹⁸ have proven to be powerful tools in investigating electronic properties, carrier capture, and escape dynamics.¹⁹ Tunnel emission from a single QW was reported several years ago by Letartre, Stievenard, and Lonoo.²⁰ The electronic properties of QD's Coulomb charging effects, and the shell structure of the few-electron ground states, have been studied by capacitance and admittance spectroscopy.²¹⁻²⁸ The frequency-dependence of the tunnel-charging process has recently been studied by Luyken *et al.*²⁹ In the present work, we present time-resolved observation of electron escape from QD's as a function of temperature and electric field. From our experiments, we identify direct and thermally activated tunneling, and determine the contributing QD levels. The results are found to be in excellent agreement with numerical calculations based on eight-band $\mathbf{k}\cdot\mathbf{p}$ theory.¹⁶

All samples investigated are GaAs *pn* diodes with a layer structure as schematically depicted in Fig. 1(a), and differ only regarding the InAs insertion. The samples were grown

by metal organic chemical vapor deposition.³⁰ On top of the highly *n*-doped GaAs substrate, a 1.6- μm Si-doped ($n = 1.7 \times 10^{16} \text{ cm}^{-3}$) GaAs buffer was deposited. Then three layers of InAs, with 2.8-nm undoped GaAs spacers on top, were grown, followed by 448-nm Si-doped ($n = 1.7 \times 10^{16} \text{ cm}^{-3}$) GaAs. After this, 650-nm Zn-doped ($p = 2.5 \times 10^{17} \text{ cm}^{-3}$) GaAs and 200-nm highly Zn-doped ($p = 1.8 \times 10^{18} \text{ cm}^{-3}$) GaAs were deposited. Using standard optical lithography and lift-off techniques Ohmic contacts were formed by evaporation and subsequent alloying of Ni-Zn-Au to the top and Ni-Au/Ge-Au to the back of the structure. Finally, mesas with a diameter of 800 μm were defined by chemical wetetching.

We fabricated one sample with three layers of InAs QD's (1.7 ML nominal layer thickness) embedded in the Si-doped ($n = 1.7 \times 10^{16} \text{ cm}^{-3}$) GaAs—in the following referred to as "A"—another sample "B" with only wetting layers (WL's), and a third sample "C" without any InAs. Because of the thin GaAs spacer (2.8 nm), the QD's in sample A grow ver-

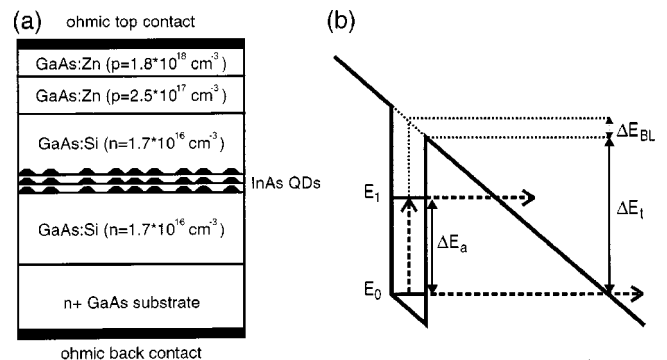


FIG. 1. Layer structure of sample A (a), and schematic conduction band of a QD along the growth direction in the presence of an electric field (b). Two electron escape mechanisms are shown; tunneling from the QD ground state E_0 into the GaAs conduction band and thermal activation into an intermediate state E_1 with subsequent tunnel emission. The electric-field-induced barrier-lowering ΔE_{BL} and the experimentally determined energies ΔE_a and ΔE_t , the activation energy and the tunnel barrier height, are also indicated.

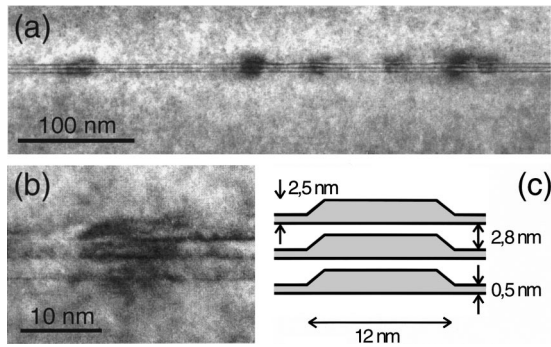


FIG. 2. Cross-section TEM in (100) direction of the triple-layer InAs QD's in GaAs matrix (a), magnification of a single QD stack (b), and average dimensions as determined from TEM images (c).

tically aligned and are electronically strongly coupled.³¹ Such a stack is expected to act as a *single* localizing potential for carriers. From cross-section transmission electron microscopy (TEM) of sample A (Fig. 2), we derive about 12 nm base width and 2.5 nm height of the QD's (assuming a truncated-pyramid shape with {101} facets), and a wetting layer (WL) thickness of about 0.5 nm. A QD sheet density of $N_{\text{OD}} = 1 \times 10^{10} \text{ cm}^{-2}$ was determined by plan-view TEM (not shown here).

The distance of the InAs insertion from the *pn* interface is chosen such that at zero bias the QD's are outside the depletion region and thus filled by electrons. At a reverse bias U_{low} below about -3.4 V, the space charge region extends over the QD layer. Carriers trapped inside the depletion region, e.g., in the QD's, are emitted with a characteristic time constant dependent on the escape mechanism. After applying filling pulses at $U_{\text{high}} > U_{\text{low}}$, the transient capacitance at reverse bias U_{low} is measured by a capacitance meter operating at a frequency of 1 MHz and recorded after A/D conversion during controlled warm-up cycles under dark conditions. The transient data sets are converted into DLTS plots using a double-boxcar correlator with a reference time constant τ_{ref} .

The photoluminescence (PL) of sample A [Fig. 3(a)] exhibits pronounced peaks from excitonic recombination in the QD's at 1.12 eV, with a full width half maximum (FWHM) of 150 meV, and in the WL system at 1.36 eV, as commonly observed in similar samples.^{10,31} In the capacitance-voltage (C-V) data of sample A [Fig. 3(b)], a plateau around -2 V is visible. Upon plotting the same data as a concentration profile [inset of Fig. 3(b)], a strong peak reflecting the carrier accumulation in the QD/WL plane, and depletion regions at both sides of the peak, become apparent. The peak position appears shifted towards larger depth by about 120 nm, since the charge on a energetic level significantly below the conduction band edge of the matrix material can only be detected for a somewhat higher reverse bias corresponding to a larger depth in the concentration profile. This is a common phenomenon known from C-V measurements of QW's.¹⁹

Typical DLTS spectra from samples A, B, and C are displayed in Fig. 4. Only the QD sample A exhibits a pronounced signal, which appears below 70 K. At higher temperatures no DLTS signal is visible, except for a peak for all three samples at about 350 K (not shown here), which is identified as the intrinsic GaAs EL2 deep level³² commonly observed in MOCVD-grown GaAs. We take the absence of

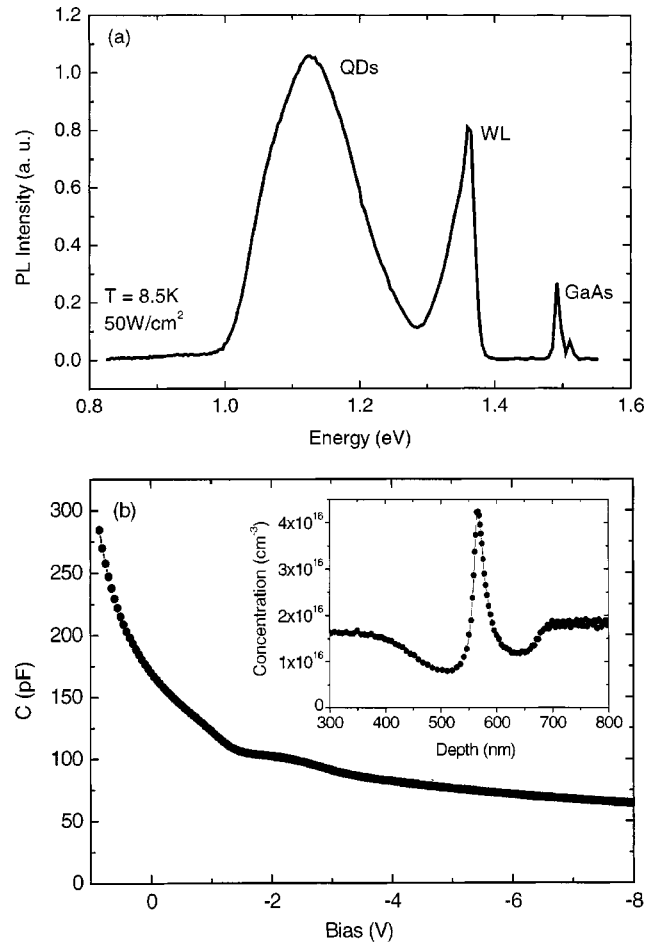


FIG. 3. Photoluminescence of the QD sample at $T = 8.5$ K (a). Capacitance-voltage data of sample A at $T = 200$ K for a measurement frequency of 1 MHz (b). The plateau in the C-V data between -1 and -3.5 V is due to carrier accumulation in the QD layer. The inset of panel (b) shows the same data as concentration profile.

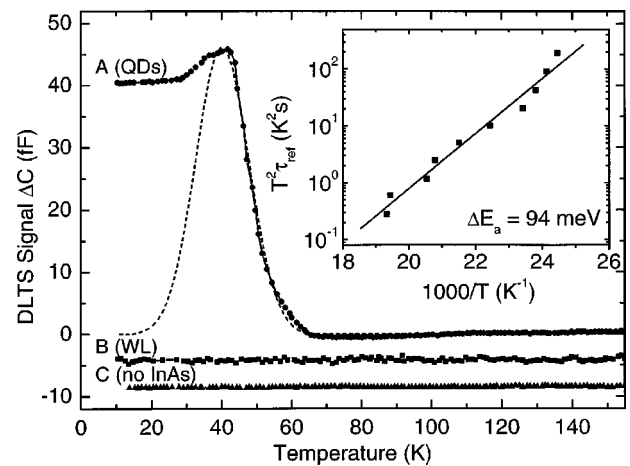


FIG. 4. DLTS signal of samples A (circles), B (squares), and C (triangles) measured at detection/pulse bias $-3.5/-0.2$ V with reference time constant $\tau_{\text{ref}} = 21$ ms. The data of samples B and C is displayed -5 and -10 fF offset, respectively. The dashed line is a fitted DLTS peak taking ensemble fluctuations in the activation energy into account. The inset shows an Arrhenius plot of the DLTS peak of sample A.

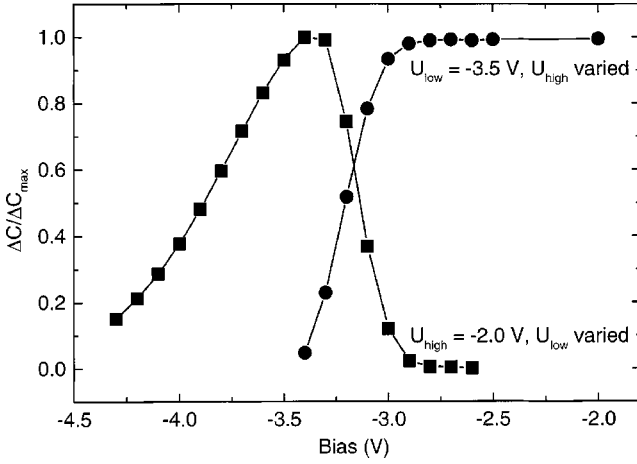


FIG. 5. DLTS depth profile. Dependence of relative DLTS peak height $\Delta C/\Delta C_{\max}$ at 40 K on detection bias (squares) for fixed filling pulse bias $U_{\text{high}} = -2.0$ V and on filling bias (circles) for fixed detection bias $U_{\text{low}} = -3.5$ V.

any further defect-related DLTS signal as an indication of high-material quality. In the following, we discuss the data of sample A.

At a temperature of about 40 K a peak, and a constant contribution below 30 K are the significant features of the DLTS signal (Fig. 4). The emission rate of a thermally activated process is usually given by¹⁸

$$e_a = \gamma T^2 \sigma_\infty \exp(-\Delta E_a/kT), \quad (1)$$

where ΔE_a is the activation energy, σ_∞ the capture cross section for $T = \infty$, and γ a temperature-independent constant. From an Arrhenius plot of the DLTS peak position for varying reference time constants τ_{ref} (inset of Fig. 4) we obtain $\sigma_\infty \approx 1 \times 10^{-11} \text{ cm}^2$ and $\Delta E_a = (94 \pm 5) \text{ meV}$.

In order to clarify the origin of the observed DLTS signal, we check the relative strength of the peak at 40 K for varying bias conditions (Fig. 5). Keeping the detection bias U_{low} fixed at -3.5 V and varying the filling pulse bias U_{high} allows us to charge an increasing part of the space charge region towards the pn interface. An increasing signal is found for filling pulse biases between -3.3 and -2.9 V; for higher bias the signal saturates, indicating that the observed electron emission is not a bulk effect, but confined to a very narrow layer. If we fix the filling pulse bias U_{high} to -2.0 V, and instead vary U_{low} , we observe a similar behavior: The DLTS signal appears for $U_{\text{low}} < -3.0$ V and has a maximum at -3.3 V. This confirms the QD layer as the origin of the emitted charge, since only for a sufficiently high-reverse bias (-3.0 V in our case) the QD's are inside the depletion region and their energy levels are lifted above the Fermi level, which leads to the observed electron emission. For $U_{\text{low}} < -3.3$ V the DLTS signal decreases again, since the relative change in capacitance, due to emission of a fixed amount of charge from the QD layer, becomes smaller because of the increasing depletion width. This behavior follows evidently from the relative DLTS peak amplitude

$$\frac{\Delta C}{C} = \frac{n_{\text{QD}} x_{\text{QD}}}{x_d^2 N_d}, \quad (2)$$

where ΔC is the DLTS peak amplitude and C the steady state capacitance at detection bias.

Fluctuations in the activation energy broaden the DLTS peak and also significantly decrease the observable peak height. From a single-peak fit with a simulated DLTS spectrum, assuming a Gaussian distribution of the activation energies (dashed line in Fig. 4), we obtain a FWHM of $(40 \pm 5) \text{ meV}$. Estimating the sheet density of the charge emitted from the QD layer from Eq. (2), using the real ΔC as given from the fit, we obtain $n_{\text{QD}} \approx 1.2 \times 10^{10} \text{ cm}^{-2}$. Taking into account the QD sheet density observed by TEM leads us to believe that the QD's are charged on average by one, maybe two electrons in our experiment.

We will now discuss the temperature-independent DLTS signal below 30 K, which can be explained by tunneling into the GaAs conduction band. Assuming a triangular barrier the tunneling rate can be written as³³

$$e_t = \frac{eE}{4\sqrt{2m^* \Delta E_t}} \exp\left(\frac{-4\sqrt{2m^* \Delta E_t}^{3/2}}{3e\hbar F}\right), \quad (3)$$

where F is the electric field, m^* the GaAs effective electron mass, and ΔE_t the barrier height. In order to estimate ΔE_t , we use as tunnel emission rate the inverse of the reference time constant for which the DLTS signal has its maximum value. We obtain an apparent barrier height of $\Delta E_t = (165 \pm 10) \text{ meV}$. As the electric field increases, the tunnel contribution is strongly enhanced and quickly dominates the DLTS signal. Therefore, the dependence of the thermally activated process on the electric field cannot be studied in our experiment. A further effect of the electric field is to be expected; namely, a reduction of barrier height, $\Delta E_{BL} = eFd_{\text{QD}}/2$, where d_{QD} is the overall thickness of the triple-QD layer. We estimate this field effect to be in the range of $\Delta E_{BL} = 23 \dots 26 \text{ meV}$ for the detection bias levels in our experiment.

The remarkable difference between the thermal activation energy ΔE_a and the estimated tunnel barrier height ΔE_t leads to our interpretation of the observed energies summarized in Fig. 1(b). We identify two different escape mechanisms; tunneling from the QD ground state into the GaAs conduction band, and thermal activation into excited QD levels with subsequent tunnel emission. The observed tunnel barrier height thus corresponds with the QD ground-state energy, and the thermal activation energy reflects the energy difference between ground and excited states. This model is supported by comparing our results with numerical simulations of the electron level scheme in our QD system based on eight-band $\mathbf{k} \cdot \mathbf{p}$ theory taking into account strain and piezoelectric effects. Details of the calculation procedure have been described elsewhere.¹⁶ For the present structure we have calculated the electron ground-state energy $E_0 = 195 \text{ meV}$ relative to the GaAs conduction band edge. This value agrees very well with $\Delta E_t + \Delta E_{BL} \approx 190 \text{ meV}$. Furthermore, the experimentally determined thermal activation energy $\Delta E_a \approx 94 \text{ meV}$ is close to the calculated energy difference between the electron ground state and the first excited state of $E_0 - E_1 = 84 \text{ meV}$.

The observation of an energetically relatively sharp DLTS peak compared to a broad PL signal is consistent with our physical picture. It even further supports the interpretation of

the thermally activated process being an intraband transition. $E_0 - E_1$ is expected to depend considerably less on ensemble fluctuations of the QD dimensions (e.g., the volume w) than the PL caused by e - h ground-state recombination, i.e., $\partial(E_0 - E_1)/\partial w \ll \partial(E_0 - \tilde{E}_0)/\partial w$, where \tilde{E}_0 denotes the hole ground-state energy (see also Fig. 4 in Ref. 16).

In conclusion, we have investigated the physics of electron escape from QD's in the presence of an external electric field. Two contributing emission mechanisms are observed: tunneling from the QD ground state into the GaAs barrier,

and thermal activation from the QD ground state into excited QD states with subsequent emission into the GaAs matrix. This scenario is found to be in good agreement with results from numerical simulations based on eight-band $\mathbf{k} \cdot \mathbf{p}$ theory of the QD level structure.

We would like to thank A. Dadgar and Z. Iqbal for stimulating discussions. One of the authors (C.K.) acknowledges financial support by "Studienstiftung des deutschen Volkes." This work was funded by DFG in the framework of SFB 296 and INTAS-RFBR program 95-IN-618.

*Also at Max-Planck-Institut für Mikrostrukturphysik, Weinberg 2, D-06120 Halle, Germany.

¹D. Bimberg, M. Grundmann, and N. N. Ledentsov, *Quantum Dot Heterostructures* (Wiley, Chichester, 1998).

²I. N. Stranski and L. Krastanow, *Sitzungsber. Akad. Wiss. Wien* **146**, 797 (1938).

³D. J. Eaglesham, and M. Cerullo, *Phys. Rev. Lett.* **64**, 1943 (1990).

⁴D. Leonard, K. Pond, and P. M. Petroff, *Phys. Rev. B* **50**, 11 687 (1994).

⁵I. Mukhametzhonov, R. Heitz, J. Zeng, P. Chen, and A. Madhukar, *Appl. Phys. Lett.* **73**, 1841 (1998).

⁶J.-Y. Marzin, J.-M. Gérard, A. Izraël, D. Barrier, and G. Bastard, *Phys. Rev. Lett.* **73**, 716 (1994).

⁷M. Grundmann, J. Christen, N. N. Ledentsov, J. Böhrer, D. Bimberg, S. S. Ruvimov, P. Werner, U. Richter, U. Gösele, J. Heydenreich, V. M. Ustinov, A. Y. Egorov, A. E. Zhukov, P. S. Kop'ev, and Z. I. Alferov, *Phys. Rev. Lett.* **74**, 4043 (1995).

⁸Y. Arakawa, and H. Sakaki, *Appl. Phys. Lett.* **40**, 939 (1982).

⁹D. Bimberg, N. Kirstaedter, N. N. Ledentsov, Z. I. Alferov, P. S. Kop'ev, and V. M. Ustinov, *IEEE J. Sel. Top. Quantum Electron.* **3**, 196 (1997).

¹⁰F. Heinrichsdorff, M.-H. Mao, N. Kirstaedter, A. Krost, D. Bimberg, A. O. Kosogov, and P. Werner, *Appl. Phys. Lett.* **71**, 22 (1997).

¹¹J. C. Campbell, D. L. Huffaker, H. Deng, and D. G. Deppe, *Electron. Lett.* **33**, 1337 (1997).

¹²S. Muto, *Jpn. J. Appl. Phys.* **34**, 210 (1995).

¹³G. Yusa and H. Sakaki, *Appl. Phys. Lett.* **70**, 345 (1997).

¹⁴J. J. Finley, M. Skalitz, M. Arzberger, A. Zrenner, G. Böhm, and G. Abstreiter, *Appl. Phys. Lett.* **73**, 2618 (1998).

¹⁵M. Grundmann, O. Stier, and D. Bimberg, *Phys. Rev. B* **52**, 11 969 (1995).

¹⁶O. Stier, M. Grundmann, and D. Bimberg, *Phys. Rev. B* **59**, 5688 (1999).

¹⁷L.-W. Wang, J. Kim, and A. Zunger, *Phys. Rev. B* **59**, 5678 (1999).

¹⁸D. V. Lang, *J. Appl. Phys.* **45**, 3023 (1974).

¹⁹P. Blood, and J. W. Orton, *The Electrical Characterization of Semiconductors: Majority Carriers and Electron States* (Academic, London, 1992), and references herein.

²⁰X. Letartre, D. Stievenard, and M. Lanoo, *J. Appl. Phys.* **69**, 7336 (1991).

²¹H. Drexler, D. Leonard, W. Hansen, J. P. Kotthaus, and P. M. Petroff, *Phys. Rev. Lett.* **73**, 2252 (1994).

²²G. Medeiros-Ribeiro, D. Leonard, and P. M. Petroff, *Appl. Phys. Lett.* **66**, 1767 (1995).

²³S. Anand, N. Carlsson, M.-E. Pistol, L. Samuelson, and W. Seifert, *Appl. Phys. Lett.* **67**, 3016 (1995).

²⁴S. Anand, N. Carlsson, M.-E. Pistol, L. Samuelson, and W. Seifert, *J. Appl. Phys.* **84**, 3747 (1998).

²⁵G. Medeiros-Ribeiro, F. G. Pikus, P. M. Petroff, and A. L. Efros, *Phys. Rev. B* **55**, 1568 (1997).

²⁶B. T. Miller, W. Hansen, S. Manus, R. J. Luyken, A. Lorke, J. P. Kotthaus, S. Huant, G. Medeiros-Ribeiro, and P. M. Petroff, *Phys. Rev. B* **56**, 6764 (1997).

²⁷P. N. Brunkov, A. Polimeni, S. T. Stoddart, M. Henini, L. Eaves, P. C. Main, A. R. Kovsh, Y. G. Musikhin, and S. G. Konnikov, *Appl. Phys. Lett.* **73**, 1092 (1998).

²⁸S. K. Zhang, H. J. Zhu, F. Lu, Z. M. Jiang, and X. Wang, *Phys. Rev. Lett.* **80**, 3340 (1998).

²⁹R. J. Luyken, A. Lorke, A. O. Govorov, J. P. Kotthaus, G. Medeiros-Ribeiro, and P. M. Petroff, *J. Appl. Phys.* **74**, 2486 (1999).

³⁰F. Heinrichsdorff, A. Krost, M. Grundmann, D. Bimberg, A. Kosogov, and P. Werner, *Appl. Phys. Lett.* **68**, 3284 (1996).

³¹N. N. Ledentsov, V. A. Shchukin, M. Grundmann, N. Kirstaedter, J. Böhrer, O. Schmidt, D. Bimberg, V. M. Ustinov, A. Y. Egorov, A. E. Zhukov, P. S. Kop'ev, S. V. Zaitsev, N. Y. Gordeev, Z. I. Alferov, A. I. Borovkov, A. O. Kosogov, S. S. Ruvimov, P. Werner, U. Gösele, and J. Heydenreich, *Phys. Rev. B* **54**, 8743 (1996).

³²J. Dabrowski and M. Scheffler, *Phys. Rev. B* **40**, 10 391 (1989).

³³G. Vincent, A. Chantre, and D. Bois, *J. Appl. Phys.* **50**, 5484 (1979).